ELSEVIER

Biophysical Chemistry 122 (2006) 101 – 113

Biophysical Chemistry

http://www.elsevier.com/locate/biophyschem

Natural terpenes: Self-assembly and membrane partitioning

A.del V. Turina [a], M.V. Nolan, J.A. Zygadlo [b], M.A. Perillo [a,*]

[a] *Biofísica-Química, Departamento de Química, Facultad de Ciencias Exactas, Físicas y Naturales, Universidad Nacional de Córdoba, Av. Vélez Sarsfield 1611, 5016 Córdoba, Argentina*

[b] *Productos Naturales, Departamento de Química, Facultad de Ciencias Exactas, Físicas y Naturales, Universidad Nacional de Córdoba, Av. Vélez Sarsfield 1611, 5016 Córdoba, Argentina*

Received 5 January 2006; received in revised form 15 February 2006; accepted 16 February 2006
Available online 6 March 2006

Abstract

Monoterpenes (MTs) are highly hydrophobic substances present in essential oils. They cover a wide spectrum of biological effects with a membrane interaction as a common point. Here we studied the surface activity of camphor, cineole, thymol, menthol and geraniol, and their ability to reach and incorporate into model membranes affecting some features of their dynamic organization. All the MTs studied self-aggregated in water with critical micellar concentrations (CMC) between 3 and 8 μM. Their octanol–water and membrane–water partition coefficients were correlated with one another. They all penetrated in monomolecular layers of dipalmitoyl-phosphatildylcholine at the air–water interface, even at surface pressures (π) above the equilibrium lateral pressure of bilayers; thymol exhibited the highest (61.3 mN/m) and camphor the lowest (37 mN/m) $\pi_{\text{cut-off}}$ value. They affected the self-aggregation of Triton X-100, increasing its CMC from 0.16 mM in the absence of MTs up to 0.68 mM (e.g. for geraniol), and the topology of sPC vesicles, increasing its surface curvature, suggesting their location at the polar head group region of the membrane. The latter was supported by their ability to increase differentially the polarity of the membrane environment sensed by two electrochromic dyes. Dipole moment values (between 1.224 and 2.523 D) and solvation areas (between 80 and 97 Å^2) were calculated from their energy-minimized structures. The relative contribution of each experimental, theoretical and structural property to determine MTs' effects on membrane dynamics were evaluated by a principal component analysis.

Keywords: Menthol; Camphor; Cineole; Geraniol; Thymol; Langmuir films penetration; Monoterpene-bilayer interaction; Self-assembling; Critical micellar concentration; Principal component analysis

1. Introduction

Monoterpenes are substances derived from isoprene hydrocarbones (2-methyl-1,3-butadiene) and originated by the attachment of two or more isoprene molecules. They are of plant origin and can exert a wide spectrum of biological actions of great importance in many different areas from food chemistry and chemical ecology to pharmacology and pharmaceutics (for a review see Ref. [1]).

The action mechanism of some terpenes involves membrane receptor-mediated effects [2–7] and stereo specificity was demonstrated in one case [6]. However, being these ones lipophilic compounds ([5] and r.f. [8]), their interaction with the hydrophobic part of the membrane induced effects on the membrane anisotropy [9,10] and dipolar organization [11]. Even if a receptor-mediated drug action could be demonstrated, in view of the dynamics of membrane organization, specificity

Abbreviations: A, absorbance; ANOVA, analysis of variance; B_{max}, maximal binding; BTB, bromothymol blue; CAM, camphor; CIN, 1,8-cineole; CMC, critical micellar concentration; *D*, dielectric constant; $\Delta\pi_0$, maximal $\Delta\pi$ determined by extrapolation to zero π_i; dpPC, dipalmitoyl-phosphatidylcholine; $GABA_A$-R, gamma aminoburic acid receptor type A form synaptosomal membranes; GER, geraniol; [^{3}H] FNZ, tritium labaled Flunitrazepam; K_d, equilibrium dissociation constant; λ_{max}, wavelength of maximal absorbance; MEN, menthol; MER, merocyanine 540; MLVs, multilamelar vesicles; MT, monoterpene; μ, molecular dipole moment; π, lateral surface pressure; $\pi_{\text{cut-off}}$, maximum value of π that allowed drug penetration in the monolayer; π_i, initial surface pressure; PCA, principal component analysis; PCs, principal components; $P_{m/w}$, membrane/water partition coefficient; $P_{o/w}$, octanol:water partition coefficient; poPC, palmitoyl-oleyl-phosphatidylcholine; SA, van der Waals area for solvation; SEM, standard error of the mean; sPC, soybean phosphatidylcholine; THY, thymol; TX-100, Triton X-100.

* Corresponding author. Fax: +54 351 4334139.
E-mail address: mperillo@enf.uncor.edu (M.A. Perillo).

0301-4622/$ - see front matter © 2006 Elsevier B.V. All rights reserved.
doi:10.1016/j.bpc.2006.02.007

becomes a relative concept because of its environmental-dependence. Thus, the reductionist perspective that considers the receptor activity and binding capacity dependent only on the interaction between two molecular entities (drug and receptor) would not be enough to describe terpenes' structure–activity relationships [12].

In pharmaceutics it is known that to maintain effective plasma concentrations of drugs as well as to reduce dose and dose-dependent toxicity, an adequate zero-order delivery is desirable. Hence, the transdermal route is a better alternative to peroral administration, which additionally provides better patient compliance. However, transdermal permeability is poor for hydrophilic drugs. In order to enhance the transdermal permeation rate of several drug molecules, oxygenated terpenes, claimed generally regarded as safe (GRAS) status, have been extensively used [13–15].

For the evaluation of the efficacy of hydrophobic drugs like terpenes, not only as permeation enhancers but also as pharmacologically active agents, drug–membrane interaction should be studied. The latter is a dynamic phenomenon, bilaterally controlled not only by the drug chemical structure but also by the membrane organization. It can be affected by drug internalization [16], and adsorption at the membrane–water interface [17] and in turn can be modified as a consequence of drug incorporation within membrane structure [18 19 20 and references therein]. Due to the nonlinear and complex behaviour of membrane lipid dynamics, the effects of drugs on membrane organization, even if they were initially subtle and local, might be amplified and spread within the membrane surface and volume [21,22].

The octanol/water partition coefficients $P_{o/w}$ have been taken as measure of drug–membrane interactions [23,24]. However, these parameters do not account for the drug binding to a tissue, a phenomenon that occurs in addition to drug partitioning. Moreover, the membrane/water partition coefficient should be taken as a resultant average value if the anisotropy and lateral domain separations in biomembranes are taken into account [25,26]. In addition, self-assembly of drug molecules will affect the thermodynamics of its partitioning towards the membrane phase.

The study of drug–membrane interactions in biomimetic systems plays an important role in the understanding of the pharmacological and pharmaceutical properties of drugs. In the present work, we studied the ability of thymol (THY), camphor (CAM), cineole (CIN), geraniol (GER) and menthol (MEN) to incorporate in model membranes and to affect their supramolecular organization in order to determine features of their particular interaction with biomembranes.

2. Materials and methods

2.1. Materials

Phospholipids were from Avanti Polar Lipids (Alabaster, AL, USA). Bromothymol blue (3′, 3″-dibromthymolsulfonephthalein) was from Sigma Co. (St. Louis, MA, USA). Merocyanine 540 (MER) was from ICN (Aurora, Ohio, USA). Monoterpenes (MT) (thymol, camphor, 1,8-cineole, geraniol and menthol) (Fig. 1) were obtained from local pharmaceutical companies and their purity was checked by Gas Chromatography using a Shimadzu GC-R1A with a flame ionisation detector and a DB-5 capillary column (30 m × 0.5 mm i.d.) at a N_2 flow rate of 0.9 ml/min. Other drugs and solvents were of analytical grade.

2.2. Determination of CMC

The CMC values of MT were determined by dispersing them in water at different final concentrations (between 0 and 58 μM) in the presence of the hydrophobic dye bromothymol blue (BTB) (80 μM final concentration). In another experiment the effect of MT on the CMC of Triton X-100 (TX-100) in water

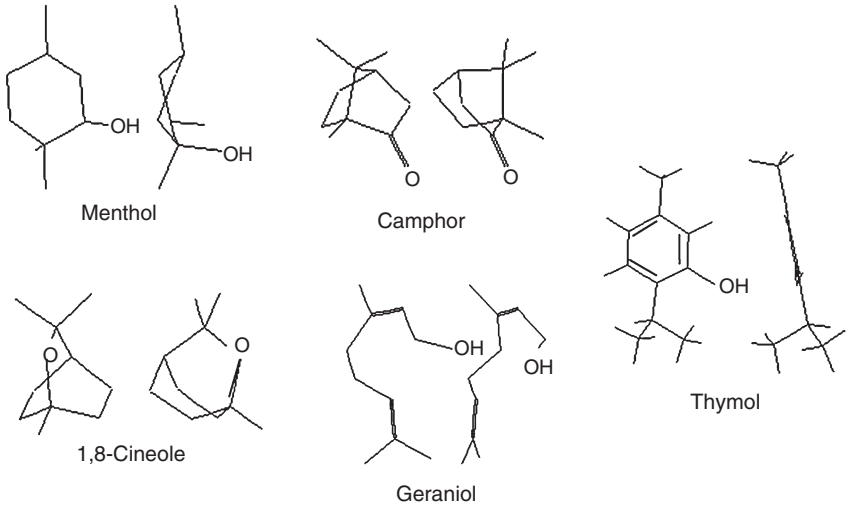

Fig. 1. Chemical structures of the monoterpenes used. Orthogonal views of the chemical structures of terpenes in the conformations of minimal energy in the vacuum. Menthol (2-(2-propyl)-5-methyl-1-cyclohexanol), camphor (1,7,7-trimethylbicyclo[2.2.1]-heptan-2-one), 1,8-cineole (1,3,3-trimethyl-2-oxabicyclo[2,2,2]octane), geraniol (3,7-dimethyl-2,6-octadien-l-ol) and thymol (5-methyl-2-(1-methylethyl)phenol).

was evaluated. In this case, the concentration of TX-100 varied between 0 and 1 mM; MTs and the hydrophobic dye were present at constant final concentrations (1 mM and 80 μM, respectively). The samples were incubated at room temperature during 10 min and then the absorbance was measured, depending on the experiment, at 437 or 485 nm (the latter was chosen to avoid TX-100 interference) with a Beckman DU 7500 spectrophotometer. The whole absorbance spectrum of BTB, which exhibited a maximum at 432 nm in water, suffered a blue-shift in low polar media, leading to an increment in the absorbance values at $\lambda < \lambda_{max}$ (wavelength with maximal absorbance) and a decrement at $\lambda > \lambda_{max}$ with respect to the values obtained in water (see Fig. 6a). Beyond the concentration of each MT or TX-100 corresponding to their particular CMC value, the absorbance of BTB at 437 nm (A_{437}) in the presence of MT reached a maximum (Fig. 2) and the A_{485} in presence of TX-100 started to decrease (Fig. 3).

2.3. Effect of monoterpenes on the size of sPC vesicles

The phospholipid was dispersed in bidistilled water at a final concentration of 2 mg/ml by a vigorous shaking during 5 min at room temperature. With this procedure we obtained multilamellar vesicles [27], which were incubated in the absence or presence of MT 0.83 mM for 1 h and then submitted to a molecular filtration gel chromatography. The chromatographic column (12 × 1 cm) was filled with Shephadex G-200; bidistilled water was used as the eluant at a 0.3 ml/min flow rate. The peaks of phospholipid vesicles were detected by using an UV detector set at 254 nm and the chromatogram was plotted with a Pharmacia XY recorder. Except for CAM, the absorbance of all the MTs assayed was zero at this wavelength [11].

2.4. Penetration of monoterpenes in monomolecular layers of dpPC at the air–water interface

Monomolecular layers were prepared and monitored as described previously [17,28]. The equipment used was a Minitrough II from KSV Instruments Ltd (Helsinki, Finland) with a circular Teflon trough (4.5 cm diameter and 0.5 cm depth). Lateral surface pressure (π) was measured by the Wihelmy plate method. Reproducibility of the values of surface pressure was ±0.001 mN/m. The aim of this experiment was to determine the maximum value of initial π that allowed drug penetration in the monolayer ($\pi_{cut\text{-}off}$). They were performed at constant surface area but at different initial surface pressures

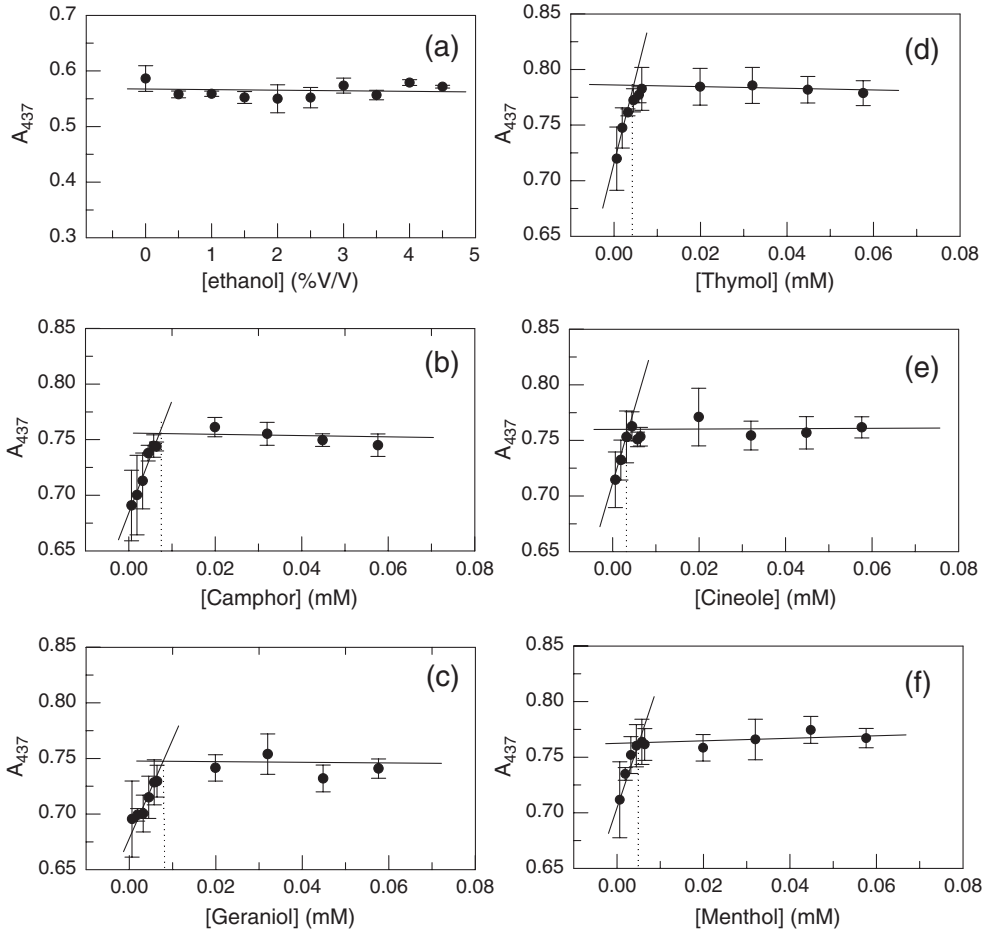

Fig. 2. Monoterpenes self-assembly in aqueous medium. Variation of the absorbance of BTB at 437 nm, with respect to the control in water, as a function of the concentration of (a) ethanol (used as MT vehicle), (b) CAM, (c) GER, (d) THY, (e) CIN, and (f) MEN. The dotted lines indicate the determination of CMC value in each case. Points represent the mean ± SEM of triplicates.

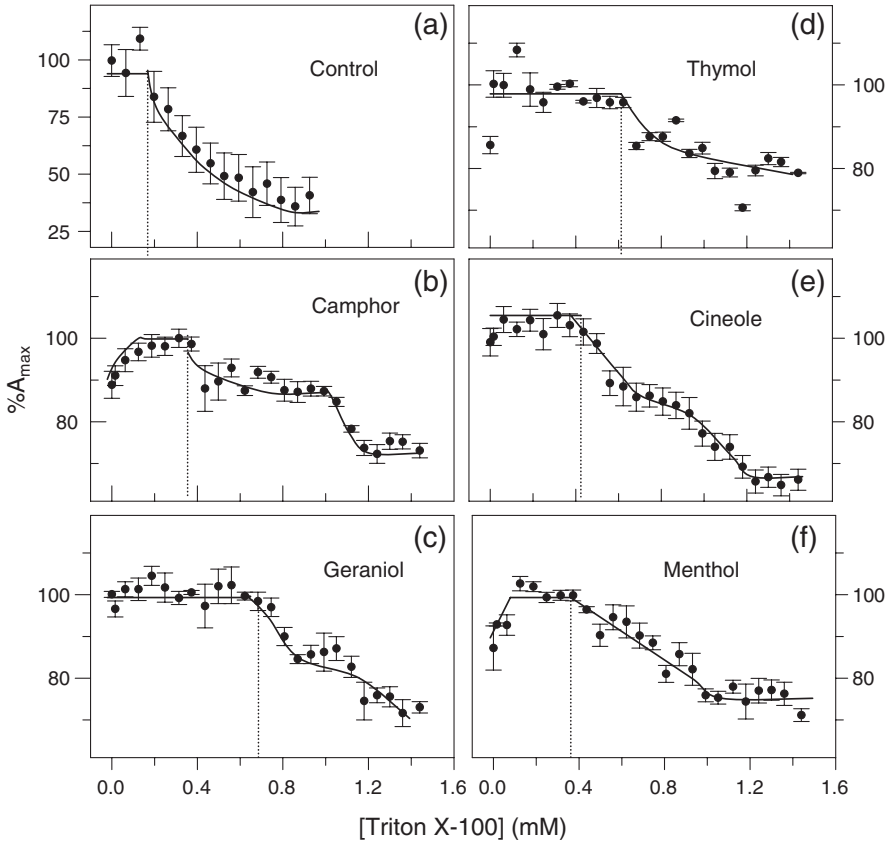

Fig. 3. Effect of monoterpenes on Triton X-100's CMC. Percentual variation of the maximal absorbance of BTB, with respect to the control in water, as a function of the concentration of Triton X-100 in the presence of monoterpenes (THY, CAM, GER, CIN 1 mM and MEN 1.6 mM). The dotted lines indicate the determination of CMC value in each case. Points represent the mean ± SEM of triplicates.

(π_i), in order to measure the changes in π ($\Delta\pi$) induced by MT penetration into the monolayer. Between 5 and 30 μl of a chloroformic solution of phospholipid were spread on an aqueous surface (bidistilled water) and about 5 min was allowed for the evaporation of chloroform and monolayer stabilization until reaching a constant baseline at the desired π_i. Then, an ethanolic solution of MT (at a final concentration of 0.5 μg/ml for THY, CAM, CIN, GER and MEN) was injected in the subphase (9 ml, 15.9 cm^2 of surface area) under continuous stirring with a miniature Teflon coated rod spinning at 150–250 rpm. The values of $\Delta\pi = \pi_{max} - \pi_i$ were plotted against π_i and the best straight line was fitted; the $\pi_{cut\text{-}off}$ was determined from the intersection of the regression line with the abscise axis and the ordinate ($\Delta\pi_0$) was taken as a measure of MT efficacy to induce the expansion of the monolayer.

2.5. Effect of monoterpenes on the polarity of a membrane environment using bromothymol blue and merocyanine as electrochromic dyes

BTB and MER solutions (80 μM and 15 μM final concentrations, respectively) were prepared in dioxane–water mixtures containing increasing dioxane proportions (0%, 20%, 45%, 70% and 82% v/v) in order to obtain media with different polarities and known values of dielectric constant (D). The absorbance spectra of BTB and MER in these solutions were recorded at intervals of 1 nm within a wavelength range between 300–700 nm, using a Beckman DU 7500 spectrophotometer equipped with a diode array detector and 0.0001 AU sensitivity. In separate experiments, the spectra of BTB and that of MER were determined in samples consisting of either *n*-octanol, aqueous dispersions of TX-100 or MT-TX-100 mixed micelles. Chemical structures and acid-base equilibrium reactions of the dyes used are shown in Scheme 1.

2.6. Determination of partition coefficients

2.6.1. Octanol/water partition coefficient

Water and *n*-octanol were pre-equilibrated overnight. After MT addition the mixture was vortexed for 5 min and incubated for an additional 15 min before centrifugation at 1000×*g* for 5 min. MT concentration was optically determined at 210 nm in the water phase and at 275 nm in the octanol phase using the corresponding ε values, and $P_{o/w} = C_o/C_w$ was calculated, where C_o and C_w are the octanol and water MT concentrations.

2.6.2. Membrane/water partition coefficient

The partition coefficient of MT between poPC multilamellar vesicles (MLVs) and water was determined by UV spectroscopy without phase separation, taking advantage of the effects of MT on the spectroscopic behaviour of MER within lipid bilayers [11]. The $P_{m/b}$ were determined essentially as described before

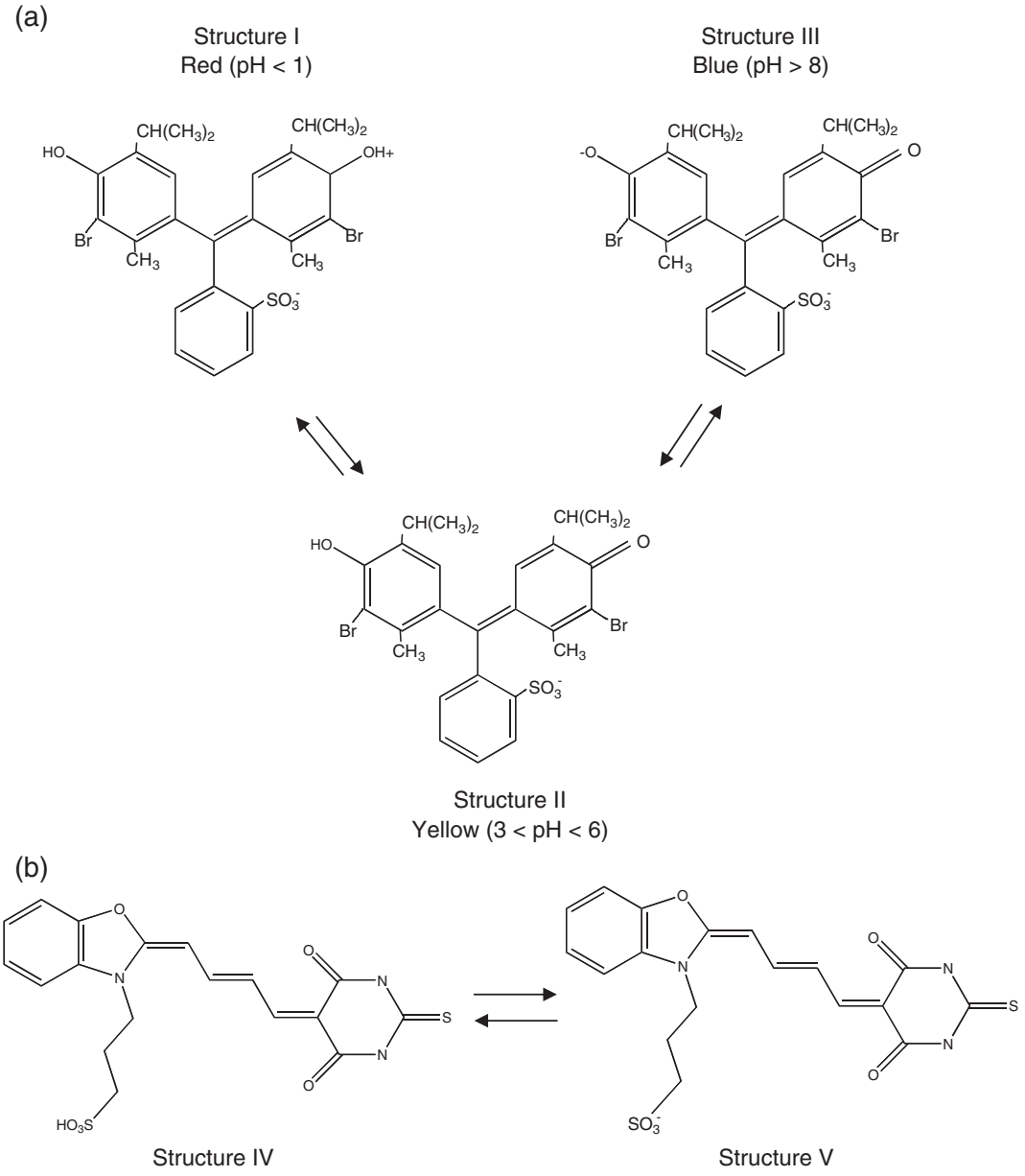

Scheme 1. Acid-base equilibrium of the electrochromic dyes. (a) Bromothymol blue: λ_{max}, structure II (BTB^-)=432 nm and structure III (BTB^{2-})=616 nm. (b) Merocyanine: protonation might occur at pH=0; in very basic media (pH=14 in NaOH), the merocyanine suffers an irreversible structural change [49].

by Pinto et al. [29] and references therein. The effect of MT on membrane organization was evaluated, at different membrane concentrations, from the changes in MER absorbance ratio A_{506}/A_{533} due to MT partition and membrane saturation. Then, for a given effect, plots of MT total concentration ($n_T=n_w+n_m$) vs. membrane volume (taken from the lipid concentration, assuming a density of 1 g/ml) gave straight lines that allowed direct $P_{m/b}$ determination from the slope/intercept ratio [29 and references therein].

2.7. Data analysis

2.7.1. Principal component analysis

Principal component analysis (PCA) was done as reported previously [25,30–32]. A multidimensional, and hence unvisualizable, swarm of points can be visualized when it is projected onto a space of fewer dimensions. This can be achieved by a rigid rotation of the original axes around the origin. The new coordinates are calculated from the equation: $\mathbf{Y}=\mathbf{U}\cdot X$ where X is the original data matrix that have been previously centred and/or standardized, $\mathbf{U}$ is an orthogonal matrix whose rows are the eigenvectors of $R=X_R\cdot X_R'$ (X_R' is the transposed of X_R) and $\mathbf{Y}$ is the matrix of the new coordinates of the data points. The new axes are known as principal axes or principal components scores. The ordination is a success if a large proportion of the total dispersion of the data is parallel with the first one, two or three principal axes. The first principal axes are oriented in such a way that the variance of the n first principal component scores is as great as possible. After PCA each

point has as coordinates not the value of each measured variable for each terpene but variously weighted sums of all the variables for each of the terpenes. The elements of the matrix **U** are the weights and, according to their values, it is possible to determine which properties have the highest influence in each principal component. Our data required standardization since the different properties were measured in non-comparable units. In order to do that the original data (x_{ij}) was centred (transformed to deviation from the respective mean of the values of each *i* property for the *j*s terpene (x_i)) and then standardized by dividing the centred data by the standard deviation of the values of the corresponding *i* property for the *j*s terpene (σ_i) by applying the following calculations to each element of the original data matrix: $(x_{ij}-x_i)/\sigma_i$.

2.7.2. Computation of molecular parameters

The software used to design the starting point molecules was Alchemy III. Energy minimization in vacuum was performed with the CS Chem3D 3.5.1 modified version of Allinger's MM2 Force Field and semi-empirical quantum mechanics calculation of dipole moments and salvation area in water was done with the MOPAC 3.5.1 module with MNDO potential function (Cambridge Soft Corporation).

2.7.3. Statistical analysis

Linear regression analysis were done by the least squares method. The data were statistically analysed using a two-tailed Student's *t*-test for independent samples or a one-way analysis of variance (ANOVA), according to the experiment [33]. The values shown represent the mean and the standard error of the mean (SEM).

3. Results

3.1. Monoterpenes' self-assembly and their effect on Triton X-100's self-aggregating structures

The self-aggregation of an amphiphilic molecule involves the appearance of a compartment with a polarity markedly different from that of water, where a hydrophobic molecule can be concentrated. In order to investigate an eventual self-assembly of MT and that of TX-100 in the presence of each MT, the changes in the absorbance of a hydrophobic dye (BTB) was evaluated as a function of the concentration of the amphiphile (each individual MT tested or TX-100). Ethanol (used as solvent for MT) did not affect the absorbance of BTB (Fig. 2a). The critical micellar concentration (CMC) was determined as the concentration of amphiphile at which the plot of absorbance vs. concentration suffered an abrupt change in its slope. The results shown in Fig. 2b–f allowed determining CMC values between 3 and 8 μM for all the MTs studied (CIN<THY<GER<MEN<CAM). On the other hand, MTs induced an increase in the CMC of TX-100 (0.16 mM, Fig. 3a) with a potency order MEN=CAM<CIN<THY<GER (Fig. 3b–f), ranging from 0.37 mM in the presence of MEN and CAM to 0.68 mM in the presence of GER. The values for the CMC of MTs as well as those for TX-100 in the presence of MTs are summarized in Table 1.

Table 1
Data matrix

Variable		Control	Thymol	Menthol	Camphor	Cineole	Geraniol
Order	Name						
1	CMC (μM)	–	4	7.5	8	3	5
2	TX-100's CMC (mM)	0.16	0.62	0.37	0.37	0.42	0.68
3	$\Delta\pi_0$ (mN/m)	3.4	18.5	12	10	8	32
4	$\pi_{\text{cut-off}}$ (mN/m)	43.5	61.3	39.5	37.0	42.6	37.5
5	Log $P_{m/b}$	–	nd	2.44	3.99	3.37	4.38
6	Log $P_{o/w}$ shake	–	3.57	nd	3.19	3.76	3.68
7	Log $P_{o/w}$ HPLC	–	nd	3.40	2.74	2.84	3.56
8	Log $P_{o/w}$ calc	–	3.30*	3.14	2.34	2.8	2.65
9	K_d (nM)	0.51	0.84	0.80	0.95	1.50	1.67
10	B_{max} (fmol/mg prot.)	736	861	1131	915	769	972
11	Linear chain	–	0	0	0	0	1
12	Aromatic ring	–	1	0	0	0	0
13	Bi-cyclic	–	0	0	1	1	0
14	OH	–	1	1	0	0	1
15	=O	–	0	0	1	0	0
16	Oxygen bridge	–	0	0	0	1	0
17	μ (Debyes)	–	1.224	1.258	2.523	1.387	1.349
18	ACS (Å^2)	–	88.82	80.75	80.89	82.77	97.40
19	*D*		42	31	28	28	32

Control samples were applied when corresponded and consisted of ([2]) an aqueous dispersion of TX-100, ([3, 4]) ethanol injected in the subphase or ([9, 10]) [^{3}H]FNZ binding to $GABA_A$-R in the absence of terpene. Variables [1–6, 17–19] present work; [7, 8] taken from Ref. [24] except the value marked as *, which was from Ref. [23]; [9, 10] taken from [48]; [17, 18] calculated as described in Section 2.7; [19] determined from λ_{max2} of BTB (Table 2). [7] Determined by an empirical relationship between the retention of solutes and therefore the capacity factor in reverse phase high performance liquid chromatography and the octanol–water partition coefficient of standard compounds; [8] calculated by the Leo and Hansch fragment method; [9, 10] determined at 0 (Control) or 2 mM MTs' concentration.

3.2. Effect of monoterpenes on the size of soybean phosphatidylcholine (sPC) vesicles

Fig. 4 shows the elution patterns of sPC vesicles in a molecular filtration gel chromatography through Sephadex G-200. The control sample (without MT) shows only one peak at the exclusion volume, the asymmetry of which suggests the existence of a certain degree of dispersion in the size of sPC vesicles. MTs induced the appearance of a second shorter peak at a higher elution volume. It is important to note that the absorbance of both sPC and MTs at the emission wavelength of the UV recorder (254 nm) were negligible. Hence, both peaks were due to light scattering. The latter peak would represent a population of vesicles of smaller size with respect to those in the former.

3.3. Penetration of monoterpenes in monomolecular layers of dpPC at the air–water interface

The penetration of MTs in the monomolecular layers of dpPC was evidenced by an increment in the surface lateral pressure at constant area. The π_i value over which penetration in the monolayer was not allowed ($\pi_{cut\text{-}off}$) was determined by extrapolating the plot of $\Delta\pi$ vs. $\pi_{initial}$ to $\Delta\pi=0$ as shown in Fig. 5. All MTs were able to penetrate from the aqueous subphase into the dpPC monolayer compressed at initial pressures well above 37 mN/m (Fig. 5, Table 1). This indicated that they were all able to penetrate bilayers, the equilibrium lateral pressure of which are around 35 mN/m [34]. On the other hand, geraniol exhibited the highest and cineole the lowest ordinate values of the $\Delta\pi$ vs. π_i plot ($\Delta\pi_0=31.89\pm1.4$ and 8.03 ± 0.82 mN/m, respectively). According to the definition given in Section 2.4 these parameters reflect their particular MT ability to deform the lipid–water interface ($\Delta\pi_0$) (Table 1).

3.4. Effect of MTs on the absorbance spectra of bromothymol blue and merocyanine

Media of different polarities were represented by solutions of decreasing dioxane concentrations. In Fig. 6c and d, the values of the local dielectric constant (D) were calibrated in terms of the position of the peaks in the absorption spectra of BTB and MER dissolved in various dioxane–water solutions (taken from Fig. 6a and b). An inspection of Scheme 1 and of the information given in its legend let us confirm that at the present experimental conditions (unbuffered water) the prevailing structures are (II) and (V). Changes in their λ_{max} could be interpreted straightforward in terms of polarity of the microenvironment, provided that no chemical irreversible change is occurring. The contrary should be said about the absorbance values which are affected not only by the polarity but also by displacements of chemical equilibria and by the partition coefficient of the individual species involved in it.

The absorbance spectra of BTB (Fig. 6a) and MER (Fig. 6b) showed that both dyes exhibit two absorbance peaks in water. In the case of BTB they are located at 336 and 432 nm. The later was associated with the mono dissociated (BTB^-) species (structure II) [35] which is the one expected to prevail at the pH assayed in the present work ($\cong 5$). Both peaks were blue-shifted with respect to water as a function of the decrease in the environmental polarity (Fig. 6c). The ratio between the absorbance values at both peaks (A_{peak1}/A_{peak2}) was almost insensitive to the dielectric constant of the solvent (Fig. 6d) but the absorbance ratio at 400 and 475 nm decreased significantly as the solvent became more polar (Fig. 6d, inset). The change in the ratio A_{400}/A_{475} for BTB is a consequence of the polarity induced blue-shift in the spectrum. Moreover, the insensitivity of A_{peak1}/A_{peak2} to D reflects that none of the acid-base equilibria involving structure II are significantly affected by BTB partitioning.

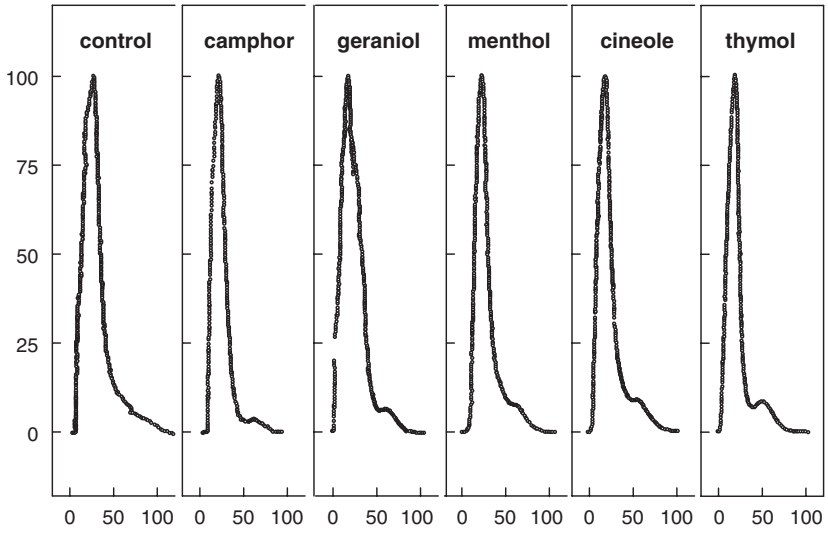

Fig. 4. Effect of monoterpenes on the size of sPC vesicles. The graph represents the elution patterns of a molecular filtration chromatography through Sephadex G-200 of a suspension of sPC vesicles previously incubated in the absence (Control) or presence of 1 mM each MT (MEN 1.6 mM).

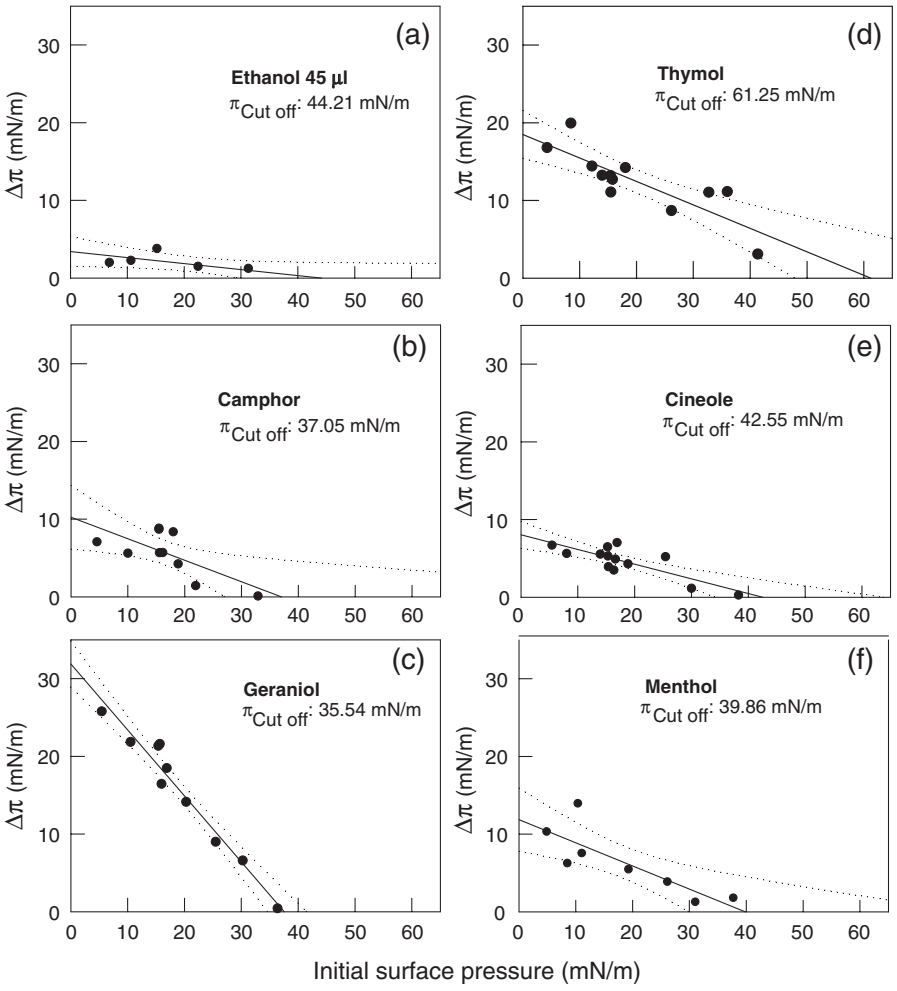

Fig. 5. Penetration of monoterpenes in monomolecular layers of dpPC at the air–water interface. In order to determine the $\pi_{cut\text{-}off}$ value, a straight line was fitted to the experimental data by a linear regression analysis.

In the case of MER in aqueous solution, one of the peaks was centred at 500 nm and the other one at 540 nm, representing the dimer and the monomer, respectively [36]. As demonstrated previously [11,37], and contrary to what happened with BTB, the decrease in the polarity of the medium induced a red-shift in MER's λ_{max2} (Fig. 6c). This behaviour as well as the increase in the ratio A_{peak1}/A_{peak2} for MER reflects the displacement of the dimer ⇆ monomer equilibrium to the right upon MER partitioning to the micelle/water interface reflecting a higher proportion of MER in the monomeric form partitioned within the less polar membrane environment.

The values of λ_{max1} and λ_{max2} of BTB and that of λ_{max2} of MER obtained in the presence of TX-100 or TX-100+MT, were interpolated in the corresponding plot of λ_{max} vs. D shown in Fig. 6c, and the values of D of the environment within the TX-100 micelles sensed by MER as well as by each BTB species, were determined (Table 2). The D values of the micellar pseudophase, estimated from the positions of the absorption peaks of BTB (λ_{max1} or λ_{max2}) and MER (λ_{max2}), were different from one another but they all were consistently higher in the presence of MTs if compared with TX-100. This indicates that each BTB species as well as MER acquired a different location within the micelle. In turn MTs induced an increase in the polarity of the media that was sensed with different sensitivity at the different dye microenvironment.

The changes in the ratio A_{peak1}/A_{peak2}, for MER, or A_{400}/A_{475}, for BTB^- induced by MTs followed the trend expected for each dye in the case of an enhancement in medium polarity, increasing for MER and decreasing for both BTB species in the presence of MT.

3.5. Monoterpenes partition coefficients

A typical experiment showing the $P_{m/w}$ determination is shown in Fig. 7. To calculate $P_{o/w}$ values the procedure explained in Section 2.6 was followed. The resulting $P_{o/w}$ and $P_{m/w}$ are shown in Table 1. The $P_{o/w}$ exhibited values very similar for all the MTs tested reflecting a hydrophobicity similar for all of them. The anisotropic organization of a bilayer membrane allowed to discriminate the significantly different behaviour of geraniol that exhibited a $P_{m/w}$ much higher than those for the other MTs. This result is consistent with its $\Delta\pi_0$ value that was also the highest among those for all the MTs. The geometry and the hydrophilic/hydrophobic compensation of the

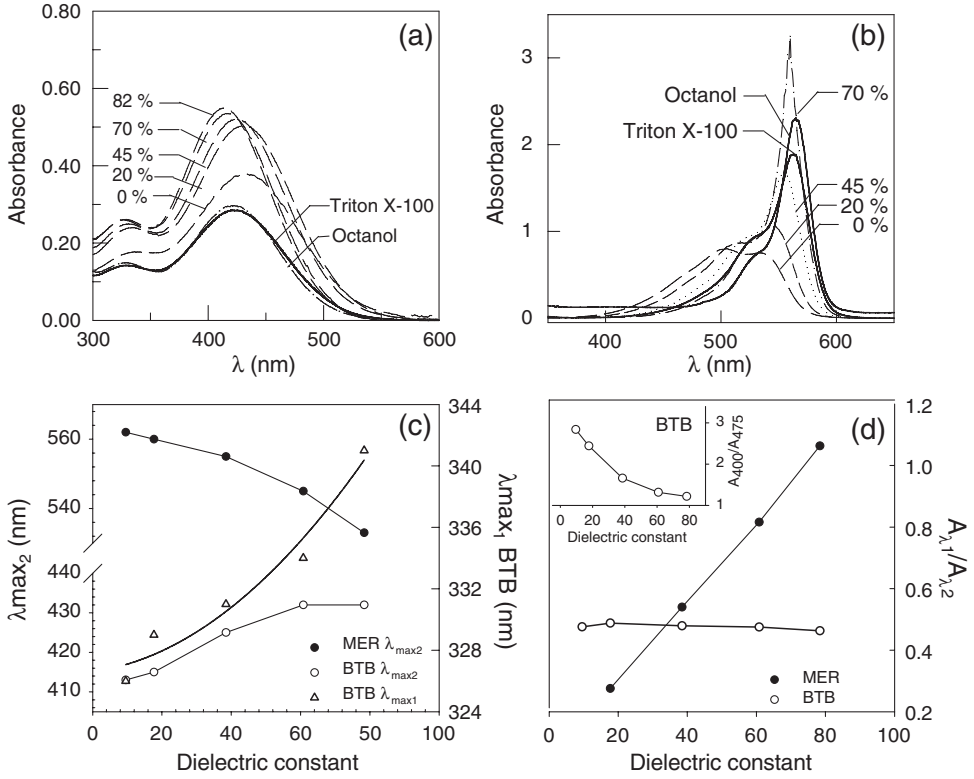

Fig. 6. Effect of polarity on the spectroscopic behaviour of the electrochromic dyes bromothymol blue and merocyanine. Absorbance spectra of BTB (a) and MER (b) in octanol, Triton X-100 and dioxane–water solutions (numbers in the graph indicate the % v/v dioxane concentrations); (c) variation of λ_{max2} for BTB (hollow circles) and MER (black circles) and (d) absorbance ratios (A_{peak1}/A_{peak2}) of BTB (white circles) and MER (black circles) as a function of D; (peak1 and peak2 were those observed at low and at high wavelength in each spectra, respectively). Inset: A_{400}/A_{475} absorbance ratio of BTB.

geraniol molecule would allow a higher thermodynamic stability and the permanence of geraniol in the bilayer. This behaviour is expressed though a higher $P_{m/w}$ value.

3.6. Principal component analysis

The understanding of the MT self-assembly and membrane interaction at the supramolecular level from physical and chemical principles opens the possibility to determine molecular features that eventually allow the prediction of particular behaviours. In order to relate the $P_{m/b}$ values to a number of another qualitative and quantitative parameters it was necessary to reduce the dimensionality of the data. For this reason a PCA was done. The data matrix used is shown in Table 1. The 84% of the total variability among MTs studied was explained by the first, second and third principal components (PCs) (Table 3). The contribution of each variable to the eigenvalues of these PCs is shown in Table 4. The eigenvector elements were scaled so that the largest element of each eigenvector was equal to unity (it is the relative, not the absolute, magnitude of the elements of an eigenvector that matters) [31]. According to which PCs made the major contribution, variables could be grouped as follows: group A (1st PC): variables 2, 3, 7, 8, 13–15, 17–19; group B (2nd PC): variables: 1, 6, 10, 16 and group C (3rd PC): 4, 5, 9, 11, 12. A graphical representation of this data is shown in Fig. 8 where a clear group can be distinguish

Table 2
Effect of monoterpenes on the spectroscopic behaviour of BTB and MER Br-thymol blue merocyanine

Sample	Br-thymol blue						Merocyanine		
	$A_{\lambda1}/A_{\lambda2}$	A_{400}/A_{475}	λ_{max1} (nm)	D_{BTB1}	λ_{max2} (nm)	D_{BTB2}	A_{dim}/A_{mon}	λ_{max} (nm)	D_{MER}
Water	0.4522	1.539	336	78	432	78	1.1018	533	78
Octanol	0.5020	2.456	329	28	420	28	0.3180	565	9
TX-100	0.4983	2.079	329	28	420	28	0.4724	565	9
TX-100+THY	0.4829[a]	1.997[a]	331	40	432	42	0.5148[a]	562	12
TX-100+MEN	0.4734[a]	1.681[a]	336	63	433	31	0.4797	563	11
TX-100+CAM	0.4903	2.082	331	40	437	28	0.5019[a]	563	11
TX-100+CIN	0.4831[a]	1.679[a]	336	63	432	28	0.4961[a]	563	11
TX-100+GER	0.4876[a]	2.069	331	40	432	32	0.4856[a]	563	11

[a] Significantly different from TX-100 (Student's t test, $p<0.05$).

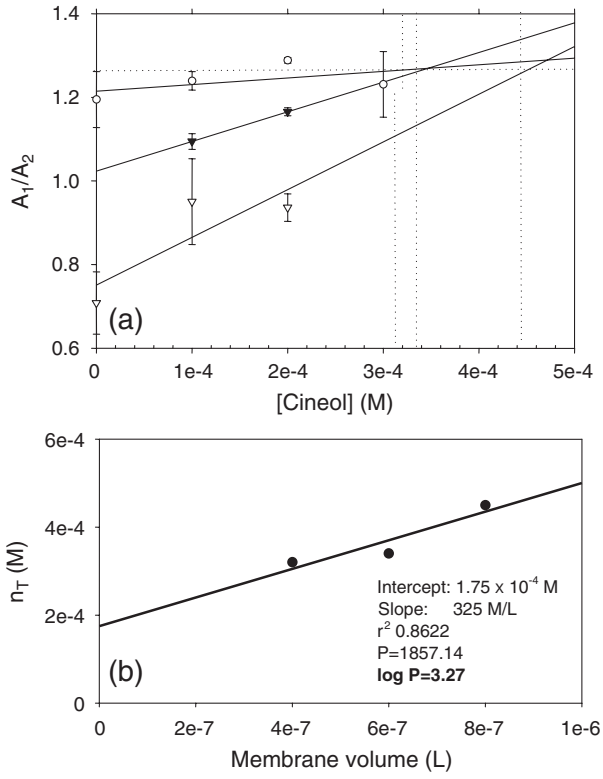

Fig. 7. Determination of monoterpenes membrane/water partition coefficient. (a) Typical experiment showing the ratio between the MER absorbance values measured at 506 and 533 nm plotted as a function of the concentration of MT in a suspension of MLVs of poPC. The phospholipid concentration varied from 2 mg/ml (top line) to 8 mg/ml (bottom line). Dotted lines show the determination of the amount of MT (n_T) required to give $A_1/A_2=1.3$ at each poPC concentration. (b) The n_T values determined from (a) were plotted against membrane volume and $P_{m/w}$ was calculated as described in Section 2.6.

composed of variables 2–4, 6, 8, 11, 12, 18, 19 as well as a close proximity between variables 15 and 17.

4. Discussion

4.1. Interaction of MT with model membranes

Amphipathic compounds are characterized by the coexistence of regions of contrasting polarity in its molecular structure. This kind of compounds, due to the hydrophobic effect, can self-aggregate spontaneously when its concentration in an aqueous media increases over a critical value named CMC. The type of the self-aggregating structure formed depends on thermodynamic and geometric restrictions associated to the hydrophilic–hydrophobic balance within the molecule. These concepts have been developed theoretically by Israelachvili [38] and then proved in many experimental systems [39 and references therein]. Due to its alicyclic chemical structure, with not flexible and not planar rings and with not clearly amphipathic structure, it is difficult to explain the self-association of MTs in micelles. Thus, piled structures, growing through a mechanism of continued association [40] or tubular three-dimensional structures [41] are more feasible. This type of structures does not have a hydrophobic compartment, the appearance of which could induce a discontinuous change in the absorbance of a hydrophobic dye partitioned in its interior.

Table 3
Principal component analysis

Principal component	Eigenvalue	Percentage	Cumulative percentage
1st	1.7726	35.35	35.45
2nd	1.3594	27.19	62.64
3rd	1.07352	21.47	84.11
4th	0.83307	16.66	100.77

Percentage, represents the total variability explained by each PC. From the first to the forth PCs accumulate the whole variability of the data analysed.

Table 4
Contribution of the individual variables to the major principal components

Variable	Principal component		
	First PC	Second PC	Third PC
CMC (μM)	−0.2302	1.0000	−0.2295
TX-100's CMC (mM)	0.7481	−0.5530	−0.2497
$\Delta\pi_0$ (mN/m)	0.7251	−0.2391	−0.6721
$\delta_{cut\text{-}off}$ (mN/m)	0.4879	−0.3461	0.9602
Log $P_{m/b}$	−0.0753	−0.4428	−0.4713
Log $P_{o/w}$ shake	0.4035	−0.5869	−0.1431
Log $P_{o/w}$ HPLC	0.7583	0.1592	−0.4869
Log $P_{o/w}$ calc	0.5358	−0.1097	−0.0748
K_d (nM)	−0.0533	−0.7539	−0.8426
B_{max} (fmol/mg prot.)	0.4024	0.9098	−0.3848
Linear chain	0.4426	−0.2805	−1.0001
Aromatic ring	0.5349	−0.2413	0.8894
Bi-cyclic	−1.0000	−0.2411	0.0706
OH	1.0000	0.2411	−0.0706
=O	−0.7309	0.3997	−0.0234
Oxygen bridge	−0.4938	−0.6950	0.1098
μ (Debyes)	−0.7872	0.3248	−0.1113
VHS (μm^3)	0.6663	−0.5014	−0.5824
D	0.7762	−0.1590	0.6616

Only the principal components with the largest eigenvalues are shown. The eigenvector elements (columns) were scaled so that the largest element of each eigenvector was equal to unity. For an explanation of variable see legend to Table 1.

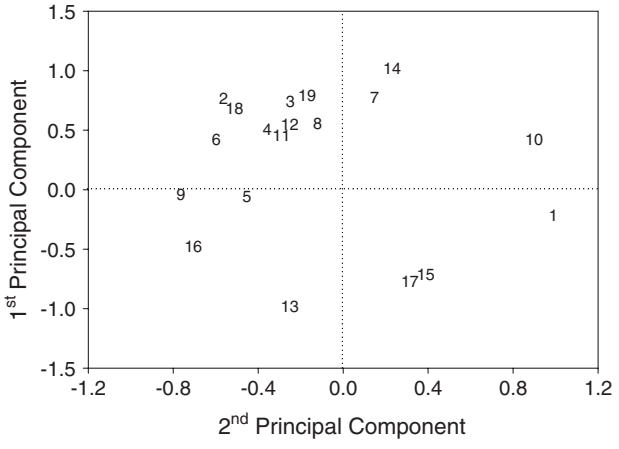

Fig. 8. Graphical representation of the principal component analysis. The first two principal components were plotted in a phase space where the grouping of related variables becomes clear. Data points are represented by the same identification numbers given to variables in Table 1.

This does not apply for GER which was the only one of the MTs studied that presented a linear hydrocarbon chain, which even being short gave the molecule a hydrophobic–hydrophilic compensation good enough to satisfy the thermodynamic and geometrical requirements to form stable monomolecular layers at the air–water interface (not shown). In spite of the differences between GER and the rest of the MTs studied, a continuous decrease in the polarity of the aqueous solution due to the increase in the concentration of all the MTs monomers led to the increment in the dye absorbance at 437 nm. Thus, the CMC of MTs (≈3–8 μM) were determined as the concentrations at which the absorbance of the hydrophobic dye BTB stopped increasing as a function of MT concentration (Fig. 2).

Conversely, TX-100 is a cone-shaped molecule able to self-assemble in micelles having a hydrophobic core [42]. Thus, the partitioning of the hydrophobic dye inside that core started at the CMC and increased at higher concentrations of TX-100 due to the growing amount of micellar structures. This was evidenced by the continuous decrement in the dye absorbance at 485 nm, which started at the detergent's CMC.

MTs induced an increment in the CMC value of TX-100 (compare Fig. 3a and b–f). Because the CMC is related with the free energy of micellation by the expression $\Delta G = R \cdot T \cdot \ln$ CMC, where $\Delta G = G_{micelle} - G_{monomer}$, in thermodynamic terms, the increment in CMC reflects either an increment in the stability of the monomer ($G_{monomer}$ decreases) or a decrement in that of the micelle ($G_{micelle}$ increases). Although none of these possibilities could be discarded, the latter was supported by other experiments (see below). Thus, MTs were able to penetrate in highly packed monomolecular layers up to a lateral surface pressure above 37 mN/m (Fig. 5). So, its penetration should be expected not only in bilayers like sPC vesicles or natural membranes whose lateral pressure is about 35 mN/m but also in micelles where the molecules are packed at even lower lateral pressures. The monolayer deformation is expressed as a change in surface pressure, depends on the initial surface pressure and is due to the combined effects of the amount of drug molecules incorporated and the individual ability of the molecular entities to induce an expansion. The latter was previously related with drug volume [28].

Once in the membrane, MTs may be located at the surface at different depths within the polar head group region, in the hydrophobic core of the micelle or in the hydrocarbon chain region of the bilayers. Independently of their localization, the presence of MTs could generate tensions and would affect the stability of the self-aggregating structure. This would be more probable if MTs were placed within the polar head group region of the amphipathic molecules (here represented by TX-100 and sPC). Drug partitioning towards a membrane generates asymmetries in membrane tensions, a condition that could lead to a curved equilibrium configuration of the membrane [21,43–45]. Our results indicated that, in the presence of MTs, bilayer vesicles were forced to acquire a higher spontaneous surface curvature and consequently a smaller size (Fig. 4) in order to attain a more relaxed state.

MER has already been used as an electrochromic dye [11,37]. The positions of the absorbance peaks of the membrane-associated MER reflected the properties of the microenvironment surrounding the dye molecules, specially the polarity if the contribution of the refractive index is small [46]. MTs induced a blue-shift with respect to TX-100 in the absorbance maximum corresponding to the monomeric (membrane bound) form of MER. This result indicated that MTs induced either an increase in the polarity (higher D) of the TX-100/water interface or a change in the dye position, within the TX-100 micelle, towards a more polar environment. In addition, the strong dipole moment of MTs, calculated from the energy minimized structure (Table 1), might have exerted repulsive electrostatic interactions with the positively charged MER, leading to the decrease in the partition coefficient of the dye as indicated by the increment in the A_{peak1}/A_{peak2} ratio (Table 2). The use of BTB led to similar conclusions in qualitative terms however, the values of D predicted a more external location of MTs within the membrane. This apparent discrepancy can be explained if we consider that what is actually being measured is the dye location and that the magnitude of the changes reflect the combined effects of the relative MTs-dye proximity, the sensitivity of the dye to sense the effects of MTs on the local dipolar potential and the sensitivity of the membrane supramolecular organization to let subtle changes grow and spread away from the initial perturbation focus. The higher effects sensed by BTB compared with MER supports the idea that MTs are located within the polar head group of membrane components.

Most of the variability between MTs was explained jointly by the first three PCs. The first principal component is a complex measure of the effect of structural, physical, chemical and pharmacological properties on the total variability of the MTs studied. Its eigenvector showed high negative loadings on the magnitude of the molecular dipole moment and the presence of bis-cycle and a keto substituent in the molecule. Conversely, this eigenvector showed high positive loadings on the change in the CMC of TX-100, the ability to deform the monolayer ($\Delta\pi_0$), the $P_{o/w}$, the presence of OH as the oxygenated substituent in the molecular structure, the solvation area which can be taken as an indirect measure of drug size and the polarity of the environment mostly affected by the drug present within the membrane. This means that the highest drug solvation favours its location in more polar environments, which are the closests to the outer membrane areas and because of this they can exert the highest membrane deformation ($\Delta\pi_0$). The opposite effects seem to be exerted by keto group in bis-cyclic molecules which confer a high dipole moment, as predicted by the positive loading of these eigenvalues to the first PC. These molecules are the smallest in size and the ones that presents the lowest $P_{o/w}$, which is consistent with opposite sign of the eigenvalues associated with these properties.

The second PC showed high positive loadings on the CMC for their self-association and on their effects on the B_{max} for ligand binding to $GABA_A$-R in synaptosomal membranes. This suggests the possibility that a certain amount of the "membrane bound" radiolabelled ligand might not be interacting with the receptor molecule but was sequestered within the MTs' self-aggregation structure and was retained in the filter during the phase separation of the membrane bound from the aqueous

phase-solubilized ligand, a possibility that has been analysed previously [47]. This calls the attention to eventual misinterpretations of binding results obtained at concentrations very high with respect to the CMC [7].

The third PC joins positive eigenvector elements for $\pi_{cut\text{-}off}$ and the presence of an aromatic ring in the molecular structure and negative loadings on $\Delta\pi_0$, $P_{m/b}$, K_d, (the highest the K_d inversely related with the binding affinity), a linear hydrocarbon chain in the molecular structure and the molecular size (related with SA). The fact that the $P_{m/b}$ were separated from the $P_{o/w}$ stresses the difference in the topology of both systems involved, one of them consisting of two liquid and isotropic phases, and on the other one being a highly anisotropic and dynamic membrane–water system. On the other hand, the ability of MTs partition into a biomembrane, expressed by its $P_{m/b}$, as well as their capacity to exert a membrane deformation, expressed by the $\Delta\pi_0$, and to modify the affinity of ligand binding to $GABA_A$-R may support the idea of the mecanosensitivity of $GABA_A$-R we observed in synaptosomal membranes submitted to different lateral surface pressures in a Langmuir–Blodgett film model [48]. In addition, it re-opens the discussion about the possibility that the results on $GABA_A$-R activity [4,6,7], might be, at least in part, a consequence of the effects of MTs on the dipolar organization of $GABA_A$-R molecular environment suggested previously [5,11].

5. Conclusions

In the present paper the interaction of monoterpenes with model membranes was studied through the aid of a group of biophysical tools involving mainly vis-spectroscopy and Langmuir films experiments. These procedures as well as the rationale involve in the interpretation of the results could be applied to analyse other drug–membrane systems. They take into account features of drug structure and physico-chemical characteristics, membrane organization and parameters describing the drug–membrane interaction phenomenon such us drug partitioning, localization, membrane expansion and changes in surface curvature. Particularly the two later reflect properties emerging from the coherent dynamics of the supramolecular arrangement which are not considered in classical pharmaceutical approaches. The application of PCA as a multivariate statistical analysis let us understand the interdependence of the parameters and some structure–activity relationships could be established (e.g. the presence of a hydroxyl and the ability to induce membrane expansion; a strong molecular dipole accompanied with low solvation area and a deeper membrane location). In addition our results points to the fact that even the claimed specific drug–membrane interactions may be modify by the drug self-assembly which will affect the binding thermodynamics from the perspective of monomeric drug disposition and will determine the occurrence of some artefacts such as the radioligand partitioning within drug self-aggregating structures. In addition, the very drug partitioning into the membrane may modulate the affinity of the drug–receptor interaction through changes in the molecular organization of membrane bound receptors surroundings.

Acknowledgements

This work was partially supported by SeCyT (Universidad Nacional de Córdoba), ANPCyT (Foncyt) and CONICET. A del V. T. and V.M.N. are fellowship holders and MAP and JAZ are career investigators of the latter institution.

References

[1] M.A. Perillo, J.A. Zygadlo. Terpenes. Stereochemistry and bioactivities. Current Topics in Phytochemistry — Research Trends. RT/PYTC/92. (in press).
[2] D.A. García, M.A. Perillo, J.A. Zygadlo, I.D. Martijena, The essential oil from *Tagetes minuta* L. modulates the binding of [3H]flunitrazepam to crude membranes from chick brain, Lipids 30 (1995) 1105.
[3] M.A. Perillo, D.A. García, R.H. Marín, J.A. Zygadlo, Tagetone modulates the coupling of Flunitrazepam and GABA binding sites ate $GABA_A$ receptor from brain membranes, Mol. Membr. Biol. 16 (1999) 189.
[4] B. Mohammadi, G. Haeseler, M. Leuwer, R. Dengler, K. Krampfl, J. Bufler, Structural requirements of phenol derivatives for direct activation of chloride currents via $GABA_A$ receptors, Eur. J. Pharmacol. 421 (2001) 85.
[5] M. Sanchez, A.del V. Turina, D.A. García, V. Nolan, M.A. Perillo, Surface activity of thymol: implications for an eventual pharmacological activity, Colloids Surf., B Biointerfaces 4 (2004) 77–86.
[6] R.E. Granger, E.L. Campbell, G.A.R. Johnston, (+)- and (−)-borneol: efficacious positive modulators of GABA action at human recombinant $\alpha_1\beta_2\gamma_{21}$. $GABA_A$ receptors, Biochem. Pharmacol. 69 (2005) 1101–1111.
[7] D.A. García, J. Bujon, C. Vale, C. Suñol, Allosteric positive interaction of thymol with the GABA(A) receptor in primary cultures of mouse cortical neurons, Neuropharmacology 50 (2005) 25–35.
[8] M.P. Zunino, J.A. Zigadlo, Changes in the composition of phospholipid fatty acids and sterols of maize root in response to monoterpenes, J. Chem. Ecol. 31 (2005) 1269–1293.
[9] A.del V. Turina, E.M. Clop, M.A. Perillo, S. Schreier, A spin label study of the interaction of biologically active terpenes with model membranes, Biocell 27 (Suppl. 1) (2003) 155.
[10] M. Bard, M.R. Albrecht, N. Gupta, C.J. Guynn, W. Stillwell, Geraniol interferes with membrane functions in strains of *Candida* and *Saccharomyces*, Lipids 23 (1988) 534–538.
[11] A.del V. Turina, M.A. Perillo, Monoterpenes control chlorodiazepoxide-membrane interaction by membrane dipole potential modifications, Biochim. Biophys. Acta 1616 (2003) 112–120.
[12] M.A. Perillo, Drug membrane interaction: its modulation at the supramolecular level, in: Condat y Baruzzi (Ed.), Recent Res. Dev. in Biophysical Chemistry, Research Singpost Ed., 2002
[13] A.H. Shojaci, M. Khan, G. Lim, R. Khosravan, Transbucal permeation of a nucleoside analog, dideoxycytidine: effects of mentol as a permeation enhancer, Int. J. Pharm. 192 (1999) 139–146.
[14] L. Kang, H.W. Jun, J.W. McCall, Physicochemical studies of lidocaine–menthol binary systems for enhanced membrane transport, Int. J. Pharm. 206 (2000) 35–42.
[15] S.T. Narishetty, R. Panchagnula, Transdermal delivery of zidovudine: effect of terpenes and their mechanism of action, J. Control. Release 95 (2004) 367–379.
[16] D.A. Garcia, M.A. Perillo, Benzodiazepine localization at the lipid–water interface: effect of membrane composition and drug chemical structure, Biochim. Biophys. Acta 1418 (1999) 221–231.
[17] D.A. Garcia, M.A. Perillo, Flunitrazepam-membrane binding and unbinding: two paths with different energy barriers, Biophys. Chem. 95 (2002) 157–164.
[18] E. de Paula, S. Schreier, Use of a novel method for determination of partition coefficients to compare the effect of local anesthetics on membrane structure, Biochim. Biophys. Acta 1240 (1995) 25–33.
[19] E. de Paula, S. Schreier, Molecular and physicochemical aspects of local anesthetic–membrane interaction, Braz. J. Med. Biol. Res. 29 (1996) 877–894.

[20] D.A. Garcia, M.A. Perillo, Effects of flunitrazepam on the Lα-HII phase transition of phosphatidylethanolamine using merocyanine 540 as a fluorescent indicator, Colloids Surf. 37 (2004) 61–69.
[21] D.A. Garcia, S. Quiroga, M.A. Perillo, Flunitrazepam partitioning into natural membranes increase surface curvature and alter cellular morphology, Chem.-Biol. Interact. 129 (2000) 263–277.
[22] L.A. Bagatolli, E. Gratton, Two-photon fluorescence microscopy of coexisting lipid domains in giant unilamellar vesicles of binary phospholipid mixtures, Biophys. J. 78 (2000) 290–305.
[23] A. Leo, C. Hansch, D. Elkins, Partition coefficients and their uses, Chem. Rev. 71 (1971) 525–616.
[24] S. Griffin, S. Grant Wyllie, J. Markham, Determination of octanol–water partition coefficient for terpenoids using reversed-phase high-performance liquid chromatography, J. Chromatogr., A 864 (1999) 221–228.
[25] M.A. Perillo, D.A. García, A. Arce, Partitioning of 1,4-benzodiazepines into natural membranes, Mol. Membr. Biol. 12 (1995) 217–224.
[26] C.M. Rosetti, R.G. Oliveira, B. Maggio, The Folch–Lees proteolipid induces phase coexistence and transverse reorganization of lateral domains in myelin monolayers, Biochim. Biophys. Acta 1668 (2005) 75–86.
[27] D. Bangham, M.W. Hill, N.G.A. Miller, Preparation and use of liposomes as models of biological membranes, in: E.D. Korn (Ed.), Methods in Membrane Biology, vol. 1, Plenum Press, New York, 1974, pp. 1–68.
[28] L. de Matos Alves Pinto, S.V. Malheiros, A.C. Lino, E. de Paula E, M.A. Perillo, Hydroxyzine, promethazine and thioridazine interaction with phospholipid monomolecular layers at the air–water interface, Biophys. Chem. 119 (2006) 247–255.
[29] L.M.A. Pinto, D.K. Yokaichiya, L.F. Fraceto, E. de Paula, Interaction of benzocaine with model membranes, Biophys. Chem. 87 (2000) 213–223.
[30] J. Crisci, M.F. López-Armengol, Introducción a la teoría y Práctica de la Taxonomía Numérica, OEA, Washington, 1983.
[31] E.C. Pielou, The Interpretation of Ecological Data, John Wiley, New York, 1984.
[32] F.J. Rohlf, Numerical Taxonomy and Multivariate Analysis System, Exeter Publishing, New York, 1984.
[33] R. Sokal, J. Rohlf, Introducción a la Bioestadística, Reverte, Barcelona, 1980.
[34] D. Marsh, Lateral pressure in membranes, Biochim. Biophys. Acta 1286 (1996) 183–223.
[35] P.M. Saikia, M. Bora, R.K. Dutta, Acid-base equilibrium of anionic dyes partially bound to micelles of non-ionic surfactants, J. Colloid Interface Sci. 285 (2005) 382–387.
[36] A.C. Biondi, E.A. Disalvo, Effect of glycerol on the interfacial properties of dipalmitoylphosphatidylcholine liposomes as measured with merocyanine 540, Biochim. Biophys. Acta 1028 (1990) 43.
[37] K. Masamoto, K. Matsuura, S. Itoh, M. Nishimura, Surface potential dependence of the distribution of charged dye molecules onto photosynthetic membranes, J. Biochem. 89 (1981) 397.
[38] J.N. Israelachvili, Intermolecular and Surface Forces, Academic Press, New York, 1989.
[39] M.A. Perillo, N.J. Scardale, R.K. Yu, B. Maggio, Modulation by gangliosides of the lamellar-inverted micelle (hexagonal II) phase transition in mixtures containing phosphatidylethanolamine and dioleoylglycerol, Proc. Natl. Acad. Sci. U. S. A. 91 (1994) 10019.
[40] P. Mukerjee, Micellar properties of drugs: micellar and nonmicellar patterns of self-association of hydrophobic solutes of different molecular structures–monomer fraction, availability, and misuses of micellar hypothesis, J. Pharm. Sci. 63 (1974) 972.
[41] W. Caetano, E.L. Gelamo, M. Tabak, R. Itri, Chlorpromazine and sodium dodecyl sulfate mixed micelles investigated by small angle X-ray scattering, J. Colloid Interface Sci. 248 (2002) 149–157.
[42] R.J. Robson, E.A. Dennis, Characterization of mixed micelles of phospholipids of various classes and a synthetic, homogeneous analogue of the nonionic detergent Triton X-100 containing nine oxyethylene groups, Biochim. Biophys. Acta 508 (1978) 513.
[43] P.R. Cullis, M.J. Hope, M.B. Bally, T.D. Madden, L.D. Mayer, D.B. Fenske, Influence of pH gradients on the transbilayer transport of drugs, lipids, peptides and metal ions into large unilamellar vesicles, Biochim. Biophys. Acta 1331 (1997) 187.
[44] M. Rasia, A. Bollini, Red blood cell shape as a function of medium's ionic strength and pH, Biochim. Biophys. Acta 1372 (1998) 198.
[45] M.A. Perillo, D.A. García, Flunitrazepam induces geometrical changes at the lipid–water interface, Colloids Surf., B Biointerfaces 20 (2001) 63.
[46] J. Lackowicz, Principles of Fluorescence Spectroscopy, Plenum Press, New York, 1983.
[47] M.A. Perillo, A. Arce, Estimation of the binding affinity constants of soluble ligand-receptor complexes by a rapid filtration technique: [3H]-flunitrazepam-bovine serum albumin as an example, J. Pharmacol. Toxicol. Methods 35 (1996) 69.
[48] A.del V. Turina, M.A. Perillo, Modulation of flunitrazepan binding to $GABA_A$-receptor induced by the molecular packing, XXXIV Annual Meeting of the Biophysical Society from Argentina, Carlos Paz, Córdoba, Argentina, 2005.
[49] A. Adenier, J.J. Aaron, A spectroscopic study of the fluorescence quenching interactions between biomedically important salts and the fluorescent probe merocyanine 540, Spectrochim. Acta, Part A 58 (2002) 543–551.